creative commons
COMMONS DEED

저작자표시-비영리-변경금지 2.0 대한민국

이용자는 아래의 조건을 따르는 경우에 한하여 자유롭게

- 이 저작물을 복제, 배포, 전송, 전시, 공연 및 방송할 수 있습니다.

다음과 같은 조건을 따라야 합니다:

저작자표시. 귀하는 원저작자를 표시하여야 합니다.

비영리. 귀하는 이 저작물을 영리 목적으로 이용할 수 없습니다.

변경금지. 귀하는 이 저작물을 개작, 변형 또는 가공할 수 없습니다.

- 귀하는, 이 저작물의 재이용이나 배포의 경우, 이 저작물에 적용된 이용허락조건을 명확하게 나타내어야 합니다.
- 저작권자로부터 별도의 허가를 받으면 이러한 조건들은 적용되지 않습니다.

저작권법에 따른 이용자의 권리는 위의 내용에 의하여 영향을 받지 않습니다.

이것은 이용허락규약(Legal Code)을 이해하기 쉽게 요약한 것입니다.

Disclaimer

dCollection

[UCI]I804:48009-200000288490

Master of Science

Synthesis and Photophysical Properties of *Ortho*-Donor-Appended TADF Compounds with Different Triarylboron Acceptors

The Graduate School of the University of Ulsan

Department of Chemistry

Hanif Mubarok

Synthesis and Photophysical Properties of *Ortho*-Donor-Appended TADF Compounds with Different Triarylboron Acceptors

Supervisor: Professor Min Hyung Lee

A Dissertation

Submitted to

The Graduate School of the University of Ulsan

In partial Fulfillment of the Requirements

For the Degree of

Master of Science

by

Hanif Mubarok

Department of Chemistry

University of Ulsan, Korea

February 2020

Synthesis and Photophysical Properties of *Ortho*-Donor-Appended TADF Compounds with Different Triarylboron Acceptors

This certifies that the dissertation of Hanif Mubarok is approved.

Committee Chair Professor Jong Wook Hong

Committee Member Professor Jaehoon Jung

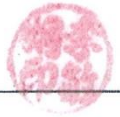

Committee Member Professor Min Hyung Lee

Department of Chemistry

University of Ulsan, Korea

February 2020

Synthesis and Photophysical Properties of *Ortho*-Donor-Appended TADF Compounds with Different Triarylboron Acceptors

Abstract:

As the development of red, green, and blue emitters are growing in display technology, thermally activated delayed fluorescence (TADF) materials have become great attention as efficient emitters in organic light emitting diodes (OLEDs) due to its ability to obtain high efficiency. However there are still problems such as lack of color purity, stability, and practical use in device. Since it was demonstrated that the acceptor moiety plays a crucial role in attaining strong TADF properties, we have been interested to investigate the effect of different acceptors in triarylboron moieties. Into the *ortho* position of phenyl ring substituted with diphenylacridine as fixed electron donor, different triarylboron acceptors, such as cyclic boraanthracene (DPAC*o*DB), oxaborin (DPAC*o*OB), as well as dimesitylboron (DPAC*o*B) were introduced to give *ortho*-donor-appended compounds. DPAC*o*DB and DPAC*o*OB which contain cyclic triarylboron showing blue-shifted emission both in toluene solution and PMMA film, compared to non-cyclic DPAC*o*B. This finding was supported by ^{11}B NMR data which shifted the cyclic compounds to the higher magnetic field and by cyclic voltammetry data related to the increasing of HOMO–LUMO gap. All compounds demonstrated high quantum efficiency (Φ_{PL} = 0.91–0.99) and displayed high thermal stability, making these compounds a good candidate as highly efficient TADF-OLED emitters.

Table of Contents

List of Figures

List of Tables

I. INTRODUCTION

1. Organic Light Emitting Diodes (OLEDs)

Organic light emitting diodes (OLEDs) is a type of light emitting diode (LED) where the emissive electroluminescent layer is composed of carbon based (organic) semiconductors, typically aromatic small molecules that emit light in response to an electric current, in contrast to the inorganic crystalline semiconductors used in traditional LEDs. Back since the first observation of organic luminescence in 1963 when Pope et al. applied a direct current to an anthracene single crystal under 400 V using silver-paste electrodes, the recent decades the field of organic electronics has progressed enormously.[1] Followed by fundamental breakthrough in 1987 when Tang and Van Slyke reported a double-layered device using tris(8-hydroxyquinoline)aluminum (Alq_3) as the emitting and electron-transporting layer. This green-emitting device showed an external quantum efficiency (EQE) of about 1% and gave electroluminescence around 1000 cd m^{-2} at driving voltages of 10 V and is still the archetypical setup for OLEDs.[2]

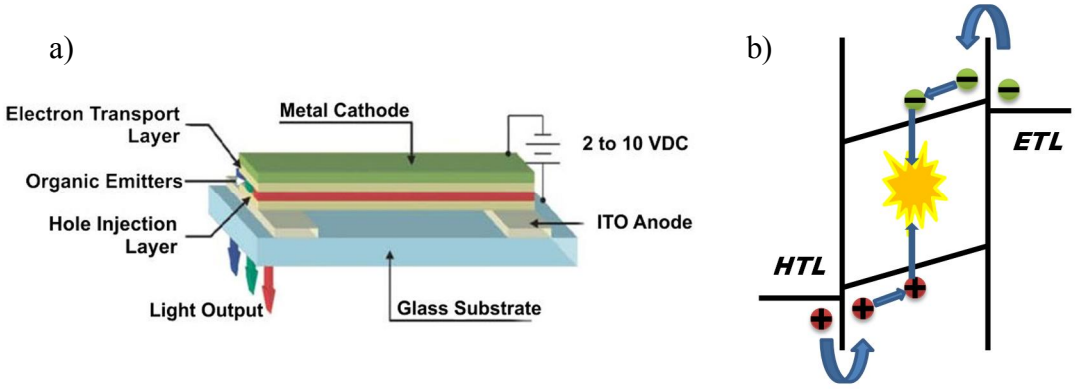

Figure 1. (a) Schematic overview of OLEDs device and (b) working principle from formation of exciton in OLEDs.

In an OLED a voltage is applied across a layer typically consist of cathode, organic emissive layer (EML), and a transparent anode (e.g. indium tin oxide ITO) resulting in the injection of electrons and holes. These electrons and holes travel through the semiconductor, before encountering each other and forming a strongly bound electron hole pair called an exciton (**Figure 1**). Under action of driving voltage, electrons are injected from the cathode into the lowest unoccupied molecular

orbital (LUMO) of the organic material. The electrons and holes move through the organic layer and recombine under the formation of an exciton capable of relaxing from its excited state to the ground state by emission of light. In addition, to provide facilitated charge injection and enhanced the recombination of electrons and holes, electron transport layer (ETL) and hole transport layer (HTL) between emissive layer were incorporated, as well as electron and hole blocking layer, giving an excellent performance of OLEDs in multilayer structure.[3]

Electrons and holes are fermions with half integer spin, and depending on the relative orientations of the two spins, the exciton can either have a total spin of zero (S = 0, singlet exciton) or a total spin of one (S = 1, triplet exciton). There are three combinations of half integer spins that form triplet exciton and only one combination which forms singlet, so that 75% of the excitons will be in the triplet state and only 25% in the singlet state.[4] This is a major issue in the creation of an efficient OLED, as radiative decay from the triplet state (T_1) to the ground state singlet (S_0) is forbidden due to conservation of angular momentum. 75% of the electrons and holes injected into the device are therefore wasted and the maximum internal quantum efficiency (IQE) of the OLED is limited to 25%. This mechanism is known as fluorescence, the 1st generation of OLED. The first solution to this problem was to incorporate heavy metals such as iridium complexes in order to increases the spin orbit coupling (SOC) between the exciton spin and orbital angular momentum, resulting in the radiative transition from the T_1 to the S_0 being no longer strictly forbidden and the T_1 state therefore becomes emissive. In addition the SOC promotes intersystem crossing (ISC) between the S_1 and the T_1 which further populates the T_1 state at the expense of the S_1. OLEDs using this mechanism are known as 2nd generation or phosphorescent OLEDs and have IQE approaching 100%.[5-6]

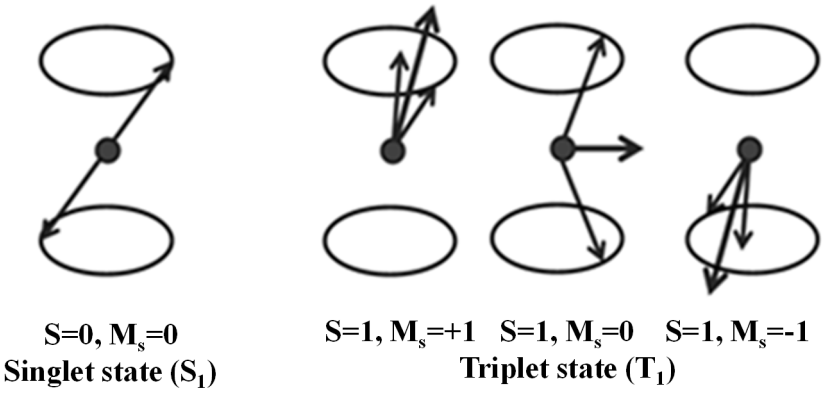

Figure 2. Spin statistic rule having singlet and triplet state.

Each pixel of an OLED display is actually made up of three separate OLEDs emitters; red, green and blue. The green and red emitters were already commercialized using cyclometalated iridium complexes materials. However, making a stable blue phosphorescent emitter has proved challenging and no suitable 2nd generation blue emitter has been found. The rarity of the heavy-metal also contributes to increased cost of the device and potential environmental contamination. Commercial displays forced to use inefficient fluorescent material and as a result, this blue emitter consumes much more power than the red and green, which is play crucial role in battery life in portable electronics. Moreover, the corresponding blue emitting materials are thus far not satisfactory in terms of their stability, color purity and brightness during device operation. Bright, deep blue and stable emitters for OLEDs are urgently needed aside from device physics, making the design and synthesis of novel blue emitter materials plays an important role in commercialization of this technology.[6]

2. Thermally Activated Delayed Fluorescence (TADF)

The 3rd generation of OLEDs, namely thermally activated delayed fluorescence (TADF) comes with promising solution to 1st and 2nd generation, that is to move away from towards fluorescent emitters and phosphorescent emitters. The first concept of TADF was reported by Perrin et al. back in 1929 and was investigated by a few others throughout the 20th century, until Adachi et al. used the TADF mechanism to create an efficient OLED without using phosphorescence in 2012.[7]

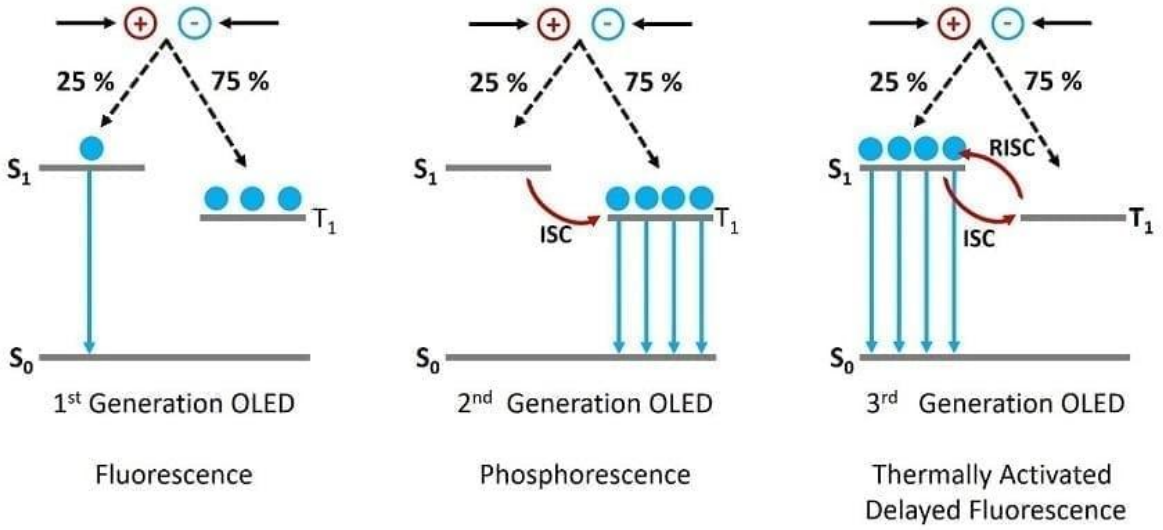

Figure 3. Generation of OLEDs.

In a TADF emitter the S_1 and T_1 levels are strongly coupled and designed with small energy difference in between (ΔE_{ST}), typically less than 0.2 eV which allows ISC between the two levels. This small energy gap enables reverse intersystem crossing (RISC) to occur, where excitons populated in the T_1 are converted back to S_1 in a thermally activated process and then can decay back to the S_0 ground state via fluorescence. Since RISC is a slow process, the fluorescence from the triplet excitons occurs later (delayed fluorescence) than from the excitons created directly in the S_1 state (prompt fluorescence).[8] A small ΔE_{ST} can be accomplished only by minimizing the electron–electron repulsion of the triplet state. From a molecular viewpoint, a spatially twisted structure usually enables a small ΔE_{ST}, because the effective separation of the HOMO and the lowest unoccupied molecular

orbital LUMO. By using the TADF mechanism, IQE of 100% can be achieved and it is hoped that TADF will allow the creation of a stable and high efficiency of blue emitter.[9]

TADF also known as E-type delayed fluorescence, is a photophysical mechanism that was first reported in 1961, when eosin was observed to emit delayed fluorescence in ethanol at 70 °C. However, the very first TADF emitters applied in OLEDs (TADF-based OLEDs) stemmed from more traditional organometallic complexes, and gradually changed from heavy metals (e.g., Ir and Pt) to lighter elements (e.g., C and N). It was in 2011 the first purely organic TADF emitter, PIC-TRZ, was reported by Adachi et.al. where the external quantum efficiency (EQE) of the OLEDs was 5.3%.[10] Following in 2012 a series of TADF emitters (4CzIPN) were reported by the same group based on donor-bridge-acceptor structure, resulting in a reduced overlap between the HOMO and the LUMO and a correspondingly small ΔE_{ST}, giving an EQE of 19.3%, which surpasses the expected theoretical maximum of 5% for EL devices employing ordinary fluorescent emitters.[7]

Design principles of organic TADF molecules mainly adopted donor (D)–acceptor (A) molecular system where the interactions between them can lead to intramolecular charge transfer (ICT) resulting in small ΔE_{ST}. Moreover, D–A molecular structure with a twist between the donor and acceptor moieties caused by bulky substituents or a spiro-junction may effectively reduce the spatial overlap of the HOMO and LUMO of the molecules, which reduces ΔE_{ST}. Several strategies related to the material parameters in order to enhance device performance were also developed i.e. the role of phenyl linker, HOMO dispersion, and dual emitting core to achieve high PLQY; frozen and rigid donor/acceptor to obtain narrow emission related to the color purity; and a stable structure to minimize efficiency roll-off.[11]

3. Triarylboron-Containing TADF Emitter

Typically donor moieties can be chosen from carbazole, amine, acridan, phenoxazine, phenithiazine, and phenazine, whereas acceptor moieties are selected from diphenyl sulfone, aromatic ketone, triazine, oxadiazole, and boron based acceptors.[11] As for boron based acceptors, triarylboron-based conjugated luminescent compounds have potential application due to their excellent photophysical and electrochemical properties. They possess a trigonal planar sp^2-hybridized trivalent boron atom with vacant p-orbital, leading to excellent electron-accepting properties and a Lewis acid in D–A organic π-conjugated system (**Figure 4**). Triarylborons with broad π-conjugate system also render p_π-π* conjugation effectively and exert a strong LUMO localization effect.[12] D–A systems with a triarylboron acceptor and amine-based donor groups have received considerable interest because of their strong ICT properties, thus strongly influences their photophysical properties, and makes them useful for non-linear optics, anion sensing, hydrogen activation and storage, optoelectronics, and TADF emitters.

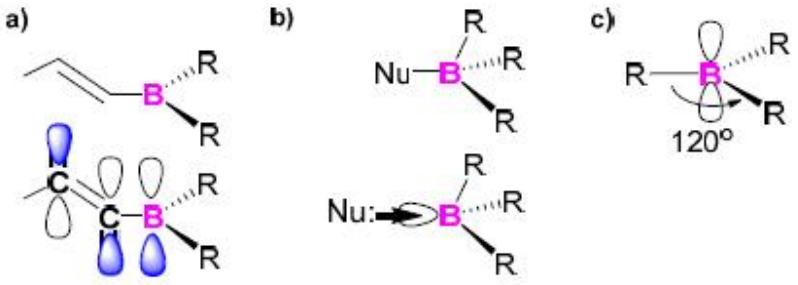

Figure 4. Essential characteristic properties of boron atom for π-conjugated materials: (a). p_π–π* conjugation; (b) Lewis acidity; and (c) trigonal planar geometry.

Many types of donor-appended triarylboron compounds have been reported. Our group has reported a series of *ortho*-donor-appended triarylboron compounds (Cz*o*B, DPA*o*B, PXZ*o*B) demonstrated highly efficient TADF emitters where Cz*o*B showed high EQE of 24.1%.[9] This series is important knowing that the *ortho* D–A connectivity and bulky nature of the triarylboron acceptor were sterically "locked" and showed a highly twisted arrangement between the donor and acceptor moieties, while their para derivatives only shows the normal fluorescence. Similar findings with

incorporation of methyl group in *meta* position of solution process non-doped OLED also shows high EQE of 19.1%.[13]

Reports of modified triarylboron acceptors are largely growing in terms of enhancing the efficiency and stability of compounds in device. In 2015, Kitamoto et. al. already reported para-donor-appended compounds consisting of 10H-phenoxaboryl group (oxaborin) as electron-accepting unit, displaying light blue and green TADF with an EQE of 15.1-22.1%.[14] Recently, Ahn et. al. reported a highly efficient deep blue TADF emitters based on symmetrical and rigid oxygen-bridged boron acceptors showing high EQE of 21.5% (TBDA-Ac).[15] Kondo et.al. also reported a narrowband deep-blue OLEDs featuring an organoboron-based emitters (*ν*-DABNA) showing Full Width at Half Maxima (FWHM) of 18 nm.[16] These findings should encouraged researchers to study and develop triarylboron-containing TADF emitters in a deep-blue region with high efficiency, high color purity, and high stability.

a)

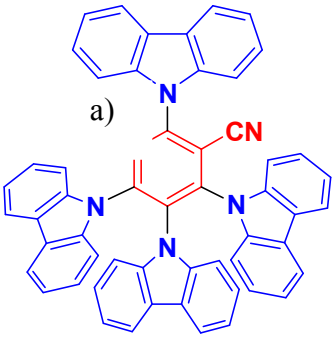

Uoyama H. et al. *Nature*, **2012**, *492*, 234.

b)

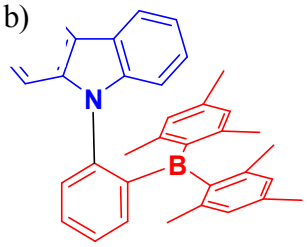

Lee, Y. H. et al. *ACS Appl. Mater. Interfaces*, **2017**, *9*, 24035

c)

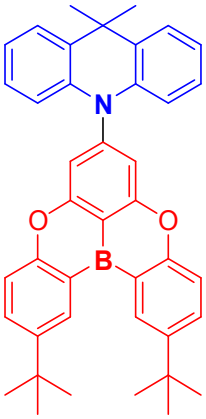

Ahn, D. H. et al. *Nat. Photonics*. **2019**, *13*, 540

d)

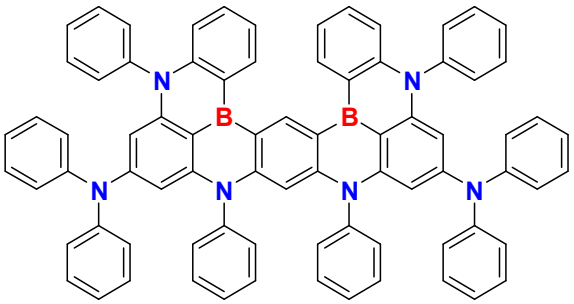

Kondo Y. et al. *Nat. Photonics*. **2019**, *13*, 678.

Figure 5. Molecular Structures of (a) 4CzIPN; (b) Cz*o*B; (c) TBDA-Ac; and (d) ν-DABNA.

4. Research Scope

Ortho donor-acceptor compounds where diphenylacridine (DPAC) as donor with cyclic cyclic triarylborons as acceptors, such as boraanthracene (DPAC*o*DB), oxaborin (DPAC*o*OB), as well as dimesitylboron (DPAC*o*B) were synthesized in several steps. In addtion, a methyl group was attached to the *ortho* position to the boryl moiety to protect the boron center from nucleophilic attack. Compounds were analyzed by NMR spectroscopy and single crystals suitable for X-ray crystallography were obtained by slow evaporation of a solution. In addition, UV-Vis absorption and emission spectra as well as emission lifetimes were measured in toluene solution and film to study the photophysical properties. From the results of X-ray crystal structure, photoluminescence (PL), and thermal stability, we describe the effects of different triarylboron acceptors on the TADF properties of *ortho* donor-acceptor compounds. All analysis was used to identify the possibility of these compounds as efficient TADF-OLEDs emitter.

II. EXPERIMENT

1. Chemical and Instrumentation

All operations were performed under an inert nitrogen atmosphere using standard Schlenk and glovebox techniques. Anhydrous grade solvents (Aldrich) were dried by passing them through an activated alumina column and stored over activated molecular sieves (5 Å). Spectrophotometric-grade solvents for photophysical measurements were used as received from Merck. Commercial reagents were used without further purification after purchase. Deuterated solvents from Cambridge isotope Laboratories were used. NMR spectra were recorded on a Bruker AM 300 (300.13 MHz for ^{1}H, 75.48 MHz for ^{13}C, 96.29 MHz for ^{11}B) at ambient temperature. Chemical shifts are given in parts per million (ppm), and are referenced against external Me_4Si (^{1}H, ^{13}C) and BF_3OEt_2 (δ 0 ppm, ^{11}B). Elemental analyses were performed on a Flash 2000 elemental analyzer (Thermo Scientific) at University of Ulsan. Cyclic voltammetry experiments were performed using an Autolab/PGSTAT101 system. Melting point (mp) was measured by Melting Point Apparatus SMP30 (Stuart Equipment).

2. Synthesis

The compounds were prepared according to **Scheme 1.** Bromo-oraanthracene (5-bromo-5,10-dihydrodibenzo[b,e]borinine) and bromo-oxaborin (5-bromo-5,10-dibenzo[b,e][1,4]oxaborinine) were prepared according to the literature procedures.[17-18] Full experimental details are given below.

2.1. 2-Bromo-1-iodo-3-methylbenzene[19]

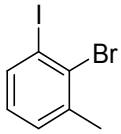

To a solution of 2-bromo-3-methylaniline (2 g, 10.75 mmol) dissolved in acetonitrile (30 mL) was added aqueous HCl (7.5 mL conc. HCl in 25 mL water), then the mixture was cooled to 0 °C, and it was added a solution of $NaNO_2$ (1.2 g, 17.43 mmol) in water (25 mL). After addition, the reaction was kept at the temperature lower than 5 °C for 30 min and it was added a solution of KI (3.62 g, 21.80 mmol) in water (50 mL). After addition, the reaction was kept at room temperature overnight, poured into water, washed with $Na_2S_2O_3$ and extracted with dichloromethane. The organic phase was dried over $MgSO_4$, and purified with silica gel

chromatography to give colorless oil (Yield: 2.4 g, 75%). ^{1}H NMR ($CDCl_3$): δ 7.70 (ddd, *J* = 7.9, 1.5, 0.6 Hz, 1H), 7.18 (ddd, *J* = 7.5, 1.5, 0.7 Hz, 1H), 6.90 (t, *J* = 7.7 Hz, 1H), 2.50 (s, 3H).

2.2. 9,9-Diphenyl-10-(2-bromo-3-methylphenyl)-9,10-dihydroacridine (DPAC*o*Br)

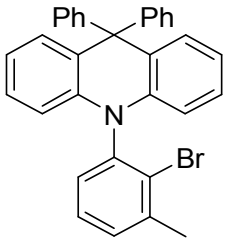

The mixture of 9,10-dihydro-9,9-diphenylacridine (0.56 g, 1.68 mmol), 2-bromo-1-iodo-3-methylbenzene (1 g, 3.37 mmol), tris-(dibenzylideneacetone)dipalladium(0) $Pd_2(dba)_3$ (0.03 g, 0.02 mmol), tri-*tert*-butylphosphine (0.02 g, 0.06 mmol), and sodium *tert*-butoxide (0.32 g, 3.36 mmol) was dissolved in dry toluene (20 mL). The reaction mixture was refluxed for 48 h. After cooling down to room temperature, the mixture was diluted with dichloromethane (20 mL), filtrated through celite pad, and concentrated under reduced pressure. The crude product was purified by silica gel column chromatography using dichloromethane/*n*-hexane (1:6, v/v) as an eluent to give DPAC*o*Br as a white solid (Yield: 0.68 g, 78%). ^{1}H NMR (CD_2Cl_2): δ 7.43-7.36 (m, 2H), 7.26 (m, 6H), 7.09-6.99 (m, 7H), 6.94-6.87 (m, 4H), 6.29 (dd, *J* = 8.6, 0.6 Hz, 2H), 2.50 (s, 3H).^{13}C NMR (CD_2Cl_2): δ 147.2, 147.0, 141.4, 140.5, 139.2, 130.7, 130.5, 130.5, 130.4, 130.3, 128.8, 128.8, 128.3, 127.6, 127.5, 127.0, 126.2, 120.3, 113.4, 56.5, 23.6. HRMS (EI) m/z Calcd for $C_{32}H_{24}BrN$, 501.1092; Found, 501.1088.

2.3. 9,9-Diphenyl-10-(2-(10H-dihydrodibenzo[b,e]borinin-10-yl)-3-methylphenyl)-9,10-dihydroacridine (DPAC*o*DB)

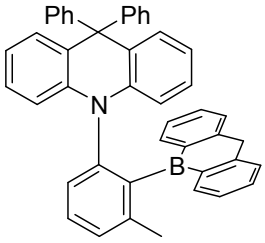

To a solution of DPAC*o*Br (0.22 g, 0.44 mmol) in dry ether (30 mL) was added dropwise *n*-BuLi (0.18 mL, 0.44 mmol) at −30 °C. The reaction mixture was allowed to warm up and stirred at room temperature for 1 h, and then 5-bromo-5,10-dihydrodibenzo[b,e]borinine (0.17 g, 0.67 mmol) in dry toluene (10 mL) was slowly added at −78 °C. After stirring at room temperature overnight, the mixture was concentrated under reduced pressure and purified by recrystallization using dichloromethane/methanol to give DPAC*o*DB as a white crystal (Yield: 0.10 g, 37%). ^{1}H NMR (CD_2Cl_2): δ 7.61 (t, *J* = 7.7 Hz, 1H), 7.47 (d, *J* = 7.5 Hz, 2H), 7.43-7.38 (m, 1H), 7.35

(td, J = 7.5, 1.5 Hz, 2H), 7.28 (d, J = 8.0 Hz, 1H), 7.22 (d, J = 7.8 Hz, 2H), 7.18-7.10 (m, 3H), 7.06-6.91 (m, 5H), 6.77-6.67 (m, 6H), 6.56 (ddd, J = 11.0, 8.2, 1.6 Hz, 4H), 6.01 (dd, J = 8.5, 1.1 Hz, 2H), 3.98 (d, J = 23.8 Hz, 1H), 3.65 (d, J = 23.7 Hz, 1H), 1.96 (s, 3H). ^{13}C NMR (CD_2Cl_2): δ 149.1, 147.5, 144.5, 142.4, 142.3, 142.1, 137.7, 132.0, 131.2, 130.4, 129.1, 128.6, 128.5, 128.3, 127.7, 127.5, 127.1, 127.1, 126.0, 126.0, 125.4, 124.3, 119.5, 115.6, 56.0, 38.0, 22.0. ^{11}B NMR (CD_2Cl_2): δ +58.2. Anal. Calcd for $C_{45}H_{34}BN$: C, 90.14; H, 5.72; N, 2.34. Found: C, 90.03; H, 5.66; N, 2.58. mp = 297 °C. T_{d5} = 324 °C.

2.4. 9,9-Diphenyl-10-(2-(10H-dibenzo[b,e][1,4]oxaborinin-10-yl)-3-methylphenyl)-9,10-dihydroacridine (DPAC*o*OB)

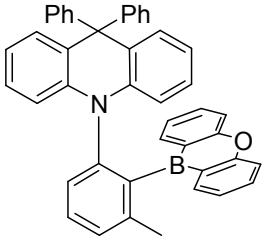

This compound was prepared in a manner analogous to the synthesis of DPAC*o*DB using DPAC*o*Br (0.30 g, 0.59 mmol), *n*-BuLi (0.24 mL, 0.60 mmol), and 5-bromo-5,10-dibenzo[b,e][1,4]oxaborinine (0.20 g, 0.78 mmol) to give DPAC*o*OB as a white crystal (Yield: 0.18 g, 50%). ^{1}H NMR (CD_2Cl_2): δ 7.64 (t, J = 7.7 Hz, 1H), 7.56-7.49 (m, 2H), 7.46 (dd, J = 7.6, 1.4 Hz, 2H), 7.41 (d, J = 7.4 Hz, 1H), 7.36-7.26 (m, 3H), 7.19-7.10 (m, 3H), 7.06 (ddd, J = 8.4, 7.3, 1.6 Hz, 2H), 6.94-6.85 (m, 3H), 6.73 (m, 6H), 6.52 (dd, J = 8.0, 1.6 Hz, 2H), 6.46-6.38 (m, 2H), 5.80 (dd, J = 8.5, 1.2 Hz, 2H), 1.91 (s, 3H). ^{13}C NMR (CD_2Cl_2): δ 158.5, 148.4, 143.8, 143.0, 142.4, 142.3, 136.0, 133.9, 131.2, 130.2, 129.4, 128.6, 128.6, 128.5, 127.2, 127.1, 126.9, 126.1, 125.7, 121.1, 119.5, 117.4, 115.2, 56.0, 22.2. ^{11}B NMR (CD_2Cl_2): δ +64.8. Anal. Calcd for $C_{44}H_{32}BNO$: C, 87.85; H, 5.36; N, 2.33. Found: C, 87.53; H, 5.28; N, 2.50. mp = 325 °C. T_{d5} = 333 °C.

2.5. 9,9-Diphenyl-10-(2-(dimesitylboryl)-3-methylphenyl)-9,10-dihydroacridine (DPAC*o*B)

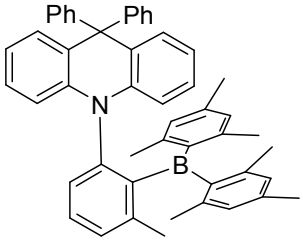

To a solution of DPAC*o*Br (0.30 g, 0.59 mmol) in dry ether (30 mL) was added dropwise *n*-BuLi (0.18 mL, 0.60 mmol) at −30 °C. The reaction mixture was allowed to warm up and stirred at room temperature for 1 h, and then dimesitylfluoroborane (Mes_2BF, 0.19 g, 0.72 mmol) in dry ether (10 mL) was slowly added at −30 °C. After stirring at room temperature

overnight, the mixture was concentrated under reduced pressure, and then purified by silica gel chromatography using dichloromethane/*n*-hexane (1:6, v/v) as an eluent. Further purification was applied by recrystallization using dichloromethane/methanol to give DPAC*o*B as a green crystal (Yield: 0.12 g, 31%). ^{1}H NMR (CD_2Cl_2): ^{1}H NMR (CD_2Cl_2) δ 7.47 (t, *J* = 7.7 Hz, 1H), 7.33-7.22 (m, 4H), 7.15-7.11 (m, 5H), 6.96 (t, *J* = 7.4 Hz, 1H), 6.89 (d, *J* = 7.8 Hz, 1H), 6.80 (t, *J* = 7.2 Hz, 1H), 6.76-6.71 (m, 2H), 6.65 (d, *J* = 9.4 Hz, 6H), 6.31 (d, *J* = 8.2 Hz, 2H), 6.06 (d, *J* = 7.1 Hz, 1H), 5.69 (s, 1H), 2.20 (s, 3H), 2.18 (s, 3H), 2.15 (s, 3H), 2.01 (s, 3H), 1.93 (s, 3H), 1.81 (s, 3H), 0.62 (s, 3H). ^{13}C NMR (CD_2Cl_2): δ 152.8, 148.1, 145.8, 143.3, 142.6, 141.9, 140.0, 138.7, 138.4, 137.2, 132.6, 131.7, 130.8, 129.9, 129.5, 128.0, 127.1, 126.3, 125.7, 125.4, 119.6, 118.8, 117.8, 117.2, 55.8, 26.0, 23.2, 22.6, 21.9, 20.6. ^{11}B NMR (CD_2Cl_2): δ +84.0. Anal. Calcd for $C_{50}H_{46}BN$: C, 89.40; H, 6.90; N, 2.09. Found: C, 89.05 ; H, 6.81 ; N, 2.28. mp = 278 °C. T_{d5} = 326 °C.

3. X-ray Crystallography

A specimen of suitable size and quality was coated with Paratone oil and mounted onto a glass capillary. The crystallographic measurement was performed using a Bruker Apex II-CCD area detector diffractometer, with graphite-monochromated MoKα radiation (λ = 0.71073 Å). The structure was solved by direct methods, and all nonhydrogen atoms were subjected to anisotropic refinement by full-matrix least-squares on F^2 by using the SHELXTL/PC package. Hydrogen atoms were placed at their geometrically calculated positions and were refined riding on the corresponding carbon atoms with isotropic thermal parameters.

4. Photophysical Measurements

UV-Vis absorption and PL spectra were recorded on a Varian Cary 100, a HORIBA FluoroMax-4P spectrophotometer and a FS5 spectrophotometer, respectively. Solution of PL spectra were obtained from oxygen-free and air-saturated toluene solutions (typically 50 μM). Absolute photoluminescence quantum yields (PLQYs, Φ_{PL}) of solutions were measured on an absolute PL

quantum yield spectrophotometer (Quantaurus-QY C11347-11, Hamamatsu Photonics) equipped with a 3.3 inch integrating sphere. Transient PL decays were measured on an FS5 spectrophotometer (Edinburgh Instruments) in either time-correlated single-photon counting (TCSPC) mode (an EPL-375 ps pulsed diode laser as a light source) or multi-channel scaling (MCS) mode (a microsecond Xenon flashlamp as a light source). The lifetimes of prompt fluorescence (τ_p) were estimated by fitting decay curves measured via the TCSPC mode, while those of delayed fluorescence (τ_d) were estimated with curves measured via the MCS mode. The temperature-dependence of PL decay was obtained with an OptistatDN^{TM} cryostat (Oxford Instruments).

5. Cyclic Voltammetry

Cyclic voltammetry measurements were carried out at room temperature in CH_2Cl_2 (1×10^{-3} M) and distilled THF (1×10^{-3} M, otherwise noted) with a three-electrode cell configuration consisting of platinum working and counter electrodes and $Ag/AgNO_3$ (0.01 M in CH_3CN) reference electrode. Tetra-*n*-butylammonium hexafluorophosphate ($TBAPF_6$ 0.1 M in CH_2Cl_2 or THF) was used as the supporting electrolyte. The redox potentials were recorded at a scan rate of 100–200 mV/s and are reported with reference to the ferrocene/ferrocenium (Fc/Fc^+) redox couple.

III. RESULT AND DISCUSSION

1. Synthesis and Characterization

A series of *ortho*-donor-appended compounds with different triarylboron acceptors (DPAC*o*DB, DPAC*o*OB, and DPAC*o*B) were prepared according to **Scheme 1**. The phenylene-linker group, 2-bromo-1-iodo-3-methylbenzene, was prepared from 2-bromo-3-methylaniline via Sandmeyer reaction.[20] The main starting precursor, DPAC*o*Br was prepared using Buchwald-Hartwig amination, selectively coupled the 9,10-dihydro-9,9-diphenylacridine (DPACH) as fixed amine donor group.[21] Prior to the final step, boraanthracene and oxaborin acceptor group were prepared according to the reported literatures.[17-18] The final *ortho*-donor-appended compounds containing triarylboron acceptors were obtained from lithiation of bromine group, followed by reaction with bromo-boraanthracene, bromo-oxaborin, and/or dimesitylboron fluoride.[9] The methyl group was introduced adjacent to the boron moiety to protect boron center from nucleophilic attack and strengthen the steric congestion between donor and acceptor. All final compounds were characterized by multinuclear NMR spectroscopy (**Figure 8-10**) and elemental analysis.

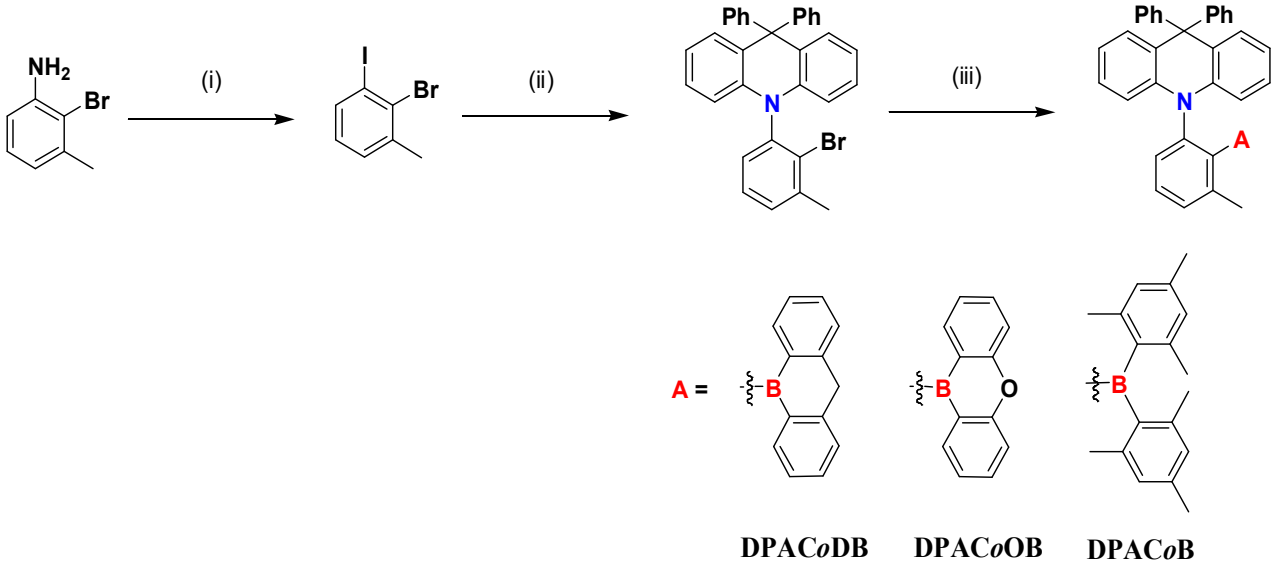

Scheme 1 . Conditions : (i) $HCl/H_2O/CH_3CN$, $NaNO_2$, then KI (ii) DPACH, $Pd_2(dba)_3$, *t*-Bu_3P, NaOtBu, toluene, reflux (iii) *n*-BuLi, Et_2O, –30 °C, then A-Br in toluene or A-F in ether (DPAC*o*B).

The ^{1}H NMR spectra of DPAC*o*DB exhibits two doublets of CH_2 group (δ 3.98 and 3.65 ppm) bridging two aryl groups in boron acceptor, whereas the ^{1}H NMR spectra of the DPAC*o*B shows sharp CH_3 peaks from $BMes_2$ group. As for ^{11}B NMR, a tri-coordinated boron center was detected as a broad singlet at δ +84.0 ppm for DPAC*o*B**,** which is consistent with the presence of trigonal planar boron center from $BMes_2$ group. In contrast with DPAC*o*DB and DPAC*o*OB which have cyclic structure, shifting to the upfield region (ca. δ +58.2 and 64.8 ppm) was observed. It can be influenced by π effects in cyclic systems when the coplanarity of the boron p_z orbital and the C=C π system is enforced, therefore increases the shielding.[22] The sterically congested nature of the *ortho* D–A structure was further confirmed by an X-ray diffraction study performed on DPAC*o*OB (**Figure 11**). A twisted structure of the compound was confirmed by a large dihedral angle of 86.45^{o} for ∠DPAC–phenylene ring and 83.69^{o} for ∠oxaborin–phenylene ring, respectively. A relative short distance between N(1) and B(1) of 2.906 Å was also observed confirming a N–B interaction for this series of compounds.[23] Furthermore, from TGA analysis (**Figure 12**) shows this series have high thermal stability, giving T_{d5} value of 324 °C, 333 °C, and 326 °C for DPAC*o*DB, DPAC*o*OB, and DPAC*o*B respectively.

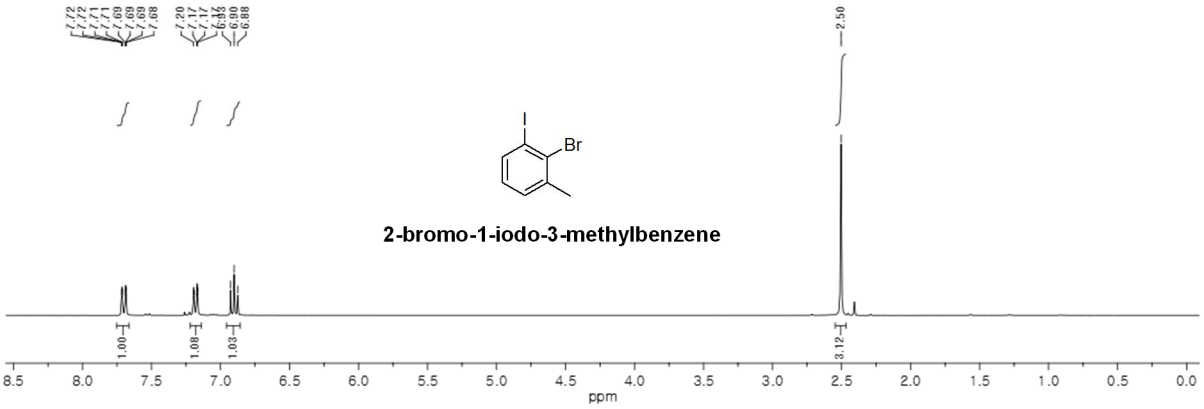

Figure 6. ^{1}H NMR spectra of 2-bromo-1-iodo-3-methylbenzene in $CDCl_3$.

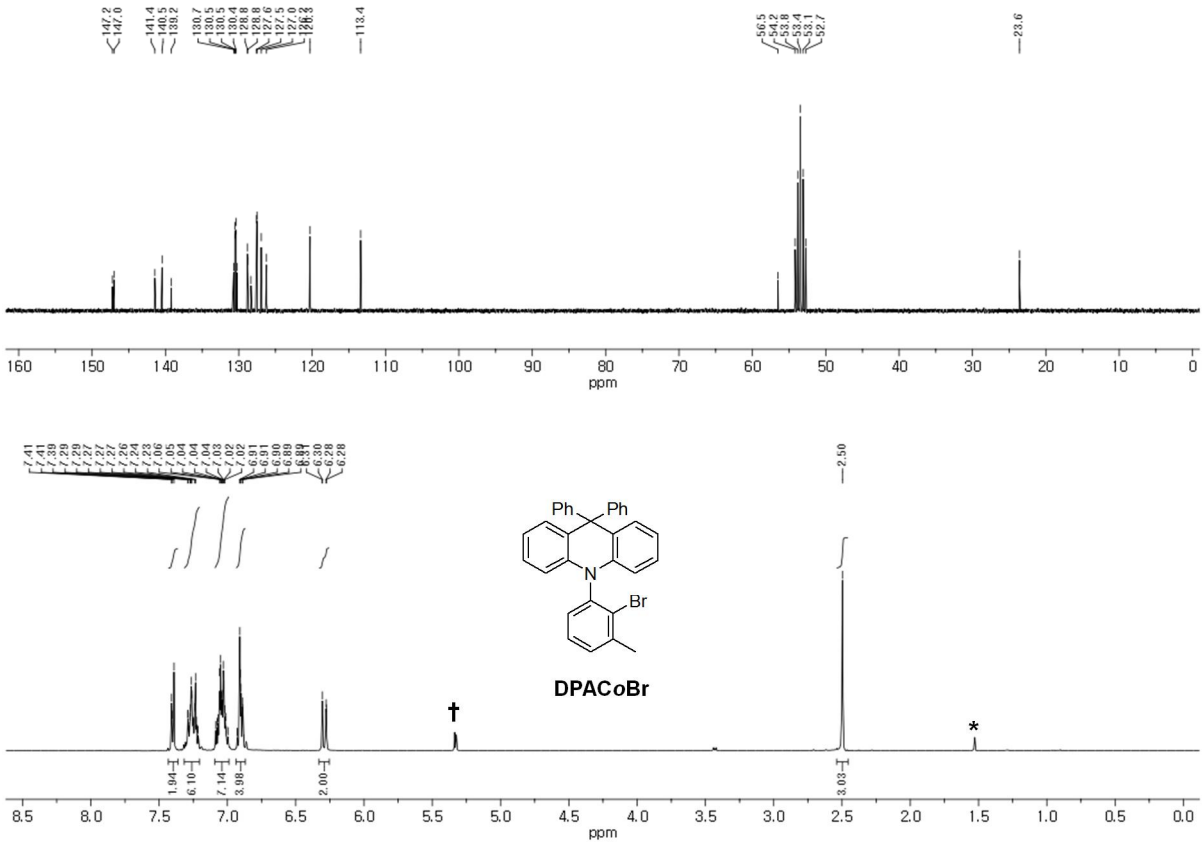

Figure 7. ^{1}H (bottom) and ^{13}C (top) NMR spectra of DPAC*o*Br in CD_2Cl_2 (* from residual H2O, † from CH_2Cl_2).

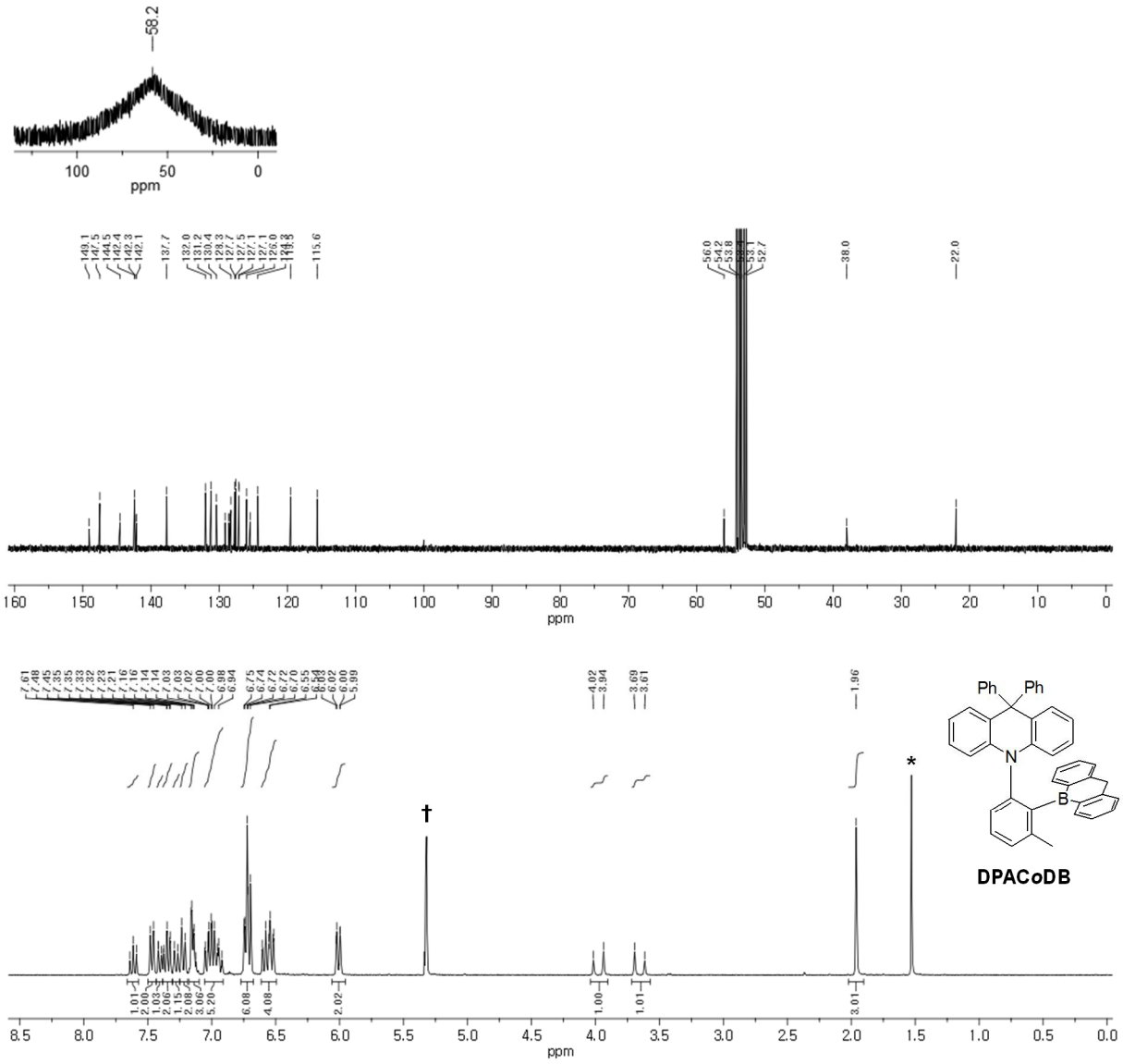

Figure 8. ^{1}H (bottom), ^{13}C (middle), and ^{11}B (top) NMR spectra of DPAC*o*DB in CD_2Cl_2 (* from residual H_2O, † from CH_2Cl_2).

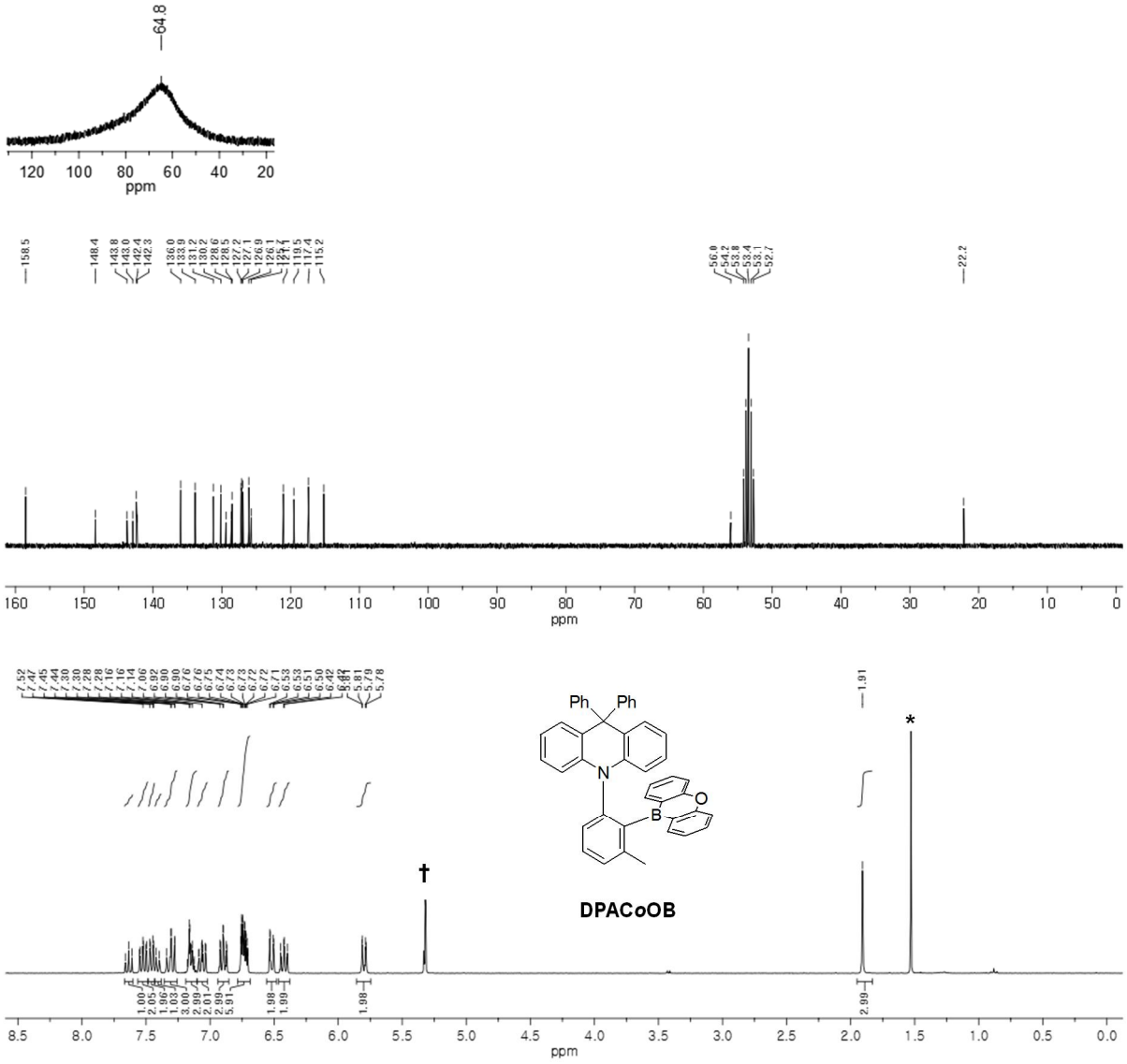

Figure 9. ^{1}H (bottom), ^{13}C (middle), and ^{11}B (top) NMR spectra of DPAC*o*OB in CD_2Cl_2 (* from residual H_2O, † from CH_2Cl_2).

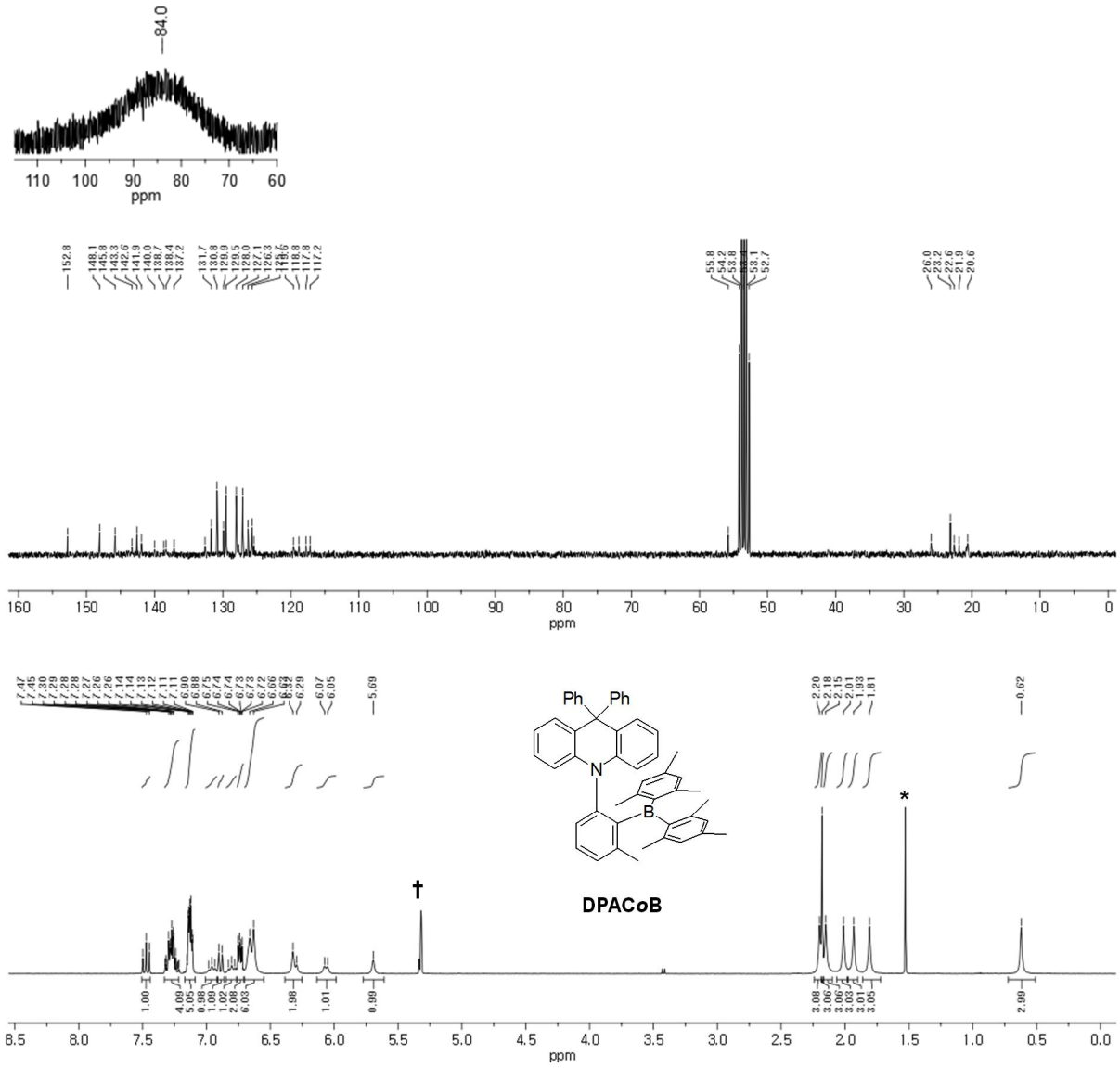

Figure 10. ^{1}H (bottom), ^{13}C (middle), and ^{11}B (top) NMR spectra of DPAC*o*B in CD_2Cl_2 (* from residual H_2O, † from CH_2Cl_2).

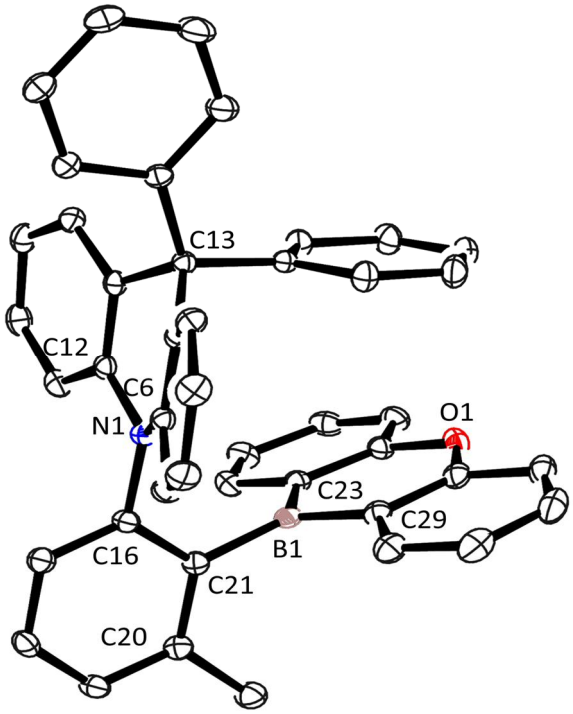

Figure 11. X-ray crystal structures DPAC*o*OB (30% thermal ellipsoids). H atoms are omitted for clarity. Color code: blue = nitrogen; brown = boron; red = oxygen.

Table 1. Selected bond lengths (Å) and angles (°) of DPAC*o*OB.

	DPAC*o*OB
Lengths(Å)	
B(1)–C(21)	1.580(3)
B(1)–C(29)	1.528(2)
N(1)–C(6)	1.412(2)
N(1)–C(16)	1.451(2)
C(16)–C(21)	1.413(2)
Angles (°)	
N(1)–C(16)–C(21)	118.0(1)
C(16)–C(21)–B(1)	121.7(1)
C(21)–B(1)–C(23)	120.4(1)
C(21)–B(1)–C(29)	124.7(1)

Table 2. Crystallographic data and parameters for DPAC*o*OB.

	DPAC*o*OB
formula	$C_{44}H_{32}BNO$
formula weight	601.51
crystal system	Triclinic
space group	*P*–1
a (Å)	9.1417(2)
b (Å)	9.5796(2)
c (Å)	19.4378(4)
α (°)	78.8745(12)
β (°)	79.0187(12)
γ (°)	74.1334(10)
V (Å^3)	1589.42(6)
Z	2
ρ_{calc} (g cm^{-3})	1.257
μ (mm^{-1})	0.074
F(000)	632
T (K)	296
hkl range	−11 → 11, −11 → 11, −23 → 23
measd reflns	20775
unique reflns [R_{int}]	5831(0.030)
reflns used for refinement	5831
refined parameters	425
R1[a] (I > 2σ(I))	0.0405
wR2[b] all data	0.1071
GOF on F^2	1.034
ρ_{fin} (max/min) (e Å^{-3})	0.176/−0.211

[a] $R1 = \sum||Fo| - |Fc||/\sum|Fo|$. [b] $wR2 = \{[\sum w(Fo^2 - Fc^2)^2]/[\sum w(Fo^2)^2]^{1/2}$

2. Photophysical Properties

The photophysical properties of all compounds, including UV/Vis absorption and photoluminescence (PL) spectra, were measured in toluene (5.0×10^{-5} M) at 298 K. (**Figure 12** and **Table 3**). The strong absorption in the high energy region of 250–350 nm can be assigned to DPAC-centered π–π* transition and the triarylboron-centered π–p_π(B) charge transfer (CT) transition.[24-25] The broad low-energy absorptions (ca. 370–400 nm) can be resulted from intramolecular charge transfer (ICT) transition from the DPAC moiety to triarylboron moiety.[24] The PL spectra shows a blue-shifted emission for cyclic triarylboron (DPAC*o*DB = 490 nm; DPAC*o*OB = 485 nm) compared to the non-cyclic $BMes_2$ (DPAC*o*B = 516 nm). This result could be associated with structural geometry of cyclic triarylboron acceptor. In cyclic triarylboron, not only the p(B)–π* interaction but also the p(B)–π interaction between B and ipso-carbon atoms effectively occur to a greater extent than non-cyclic $BMes_2$.[17] This extension of π-donating effect may contribute to raise the LUMO level and it was also explained by ^{11}B NMR featured broad signal at higher magnetic field (DPAC*o*DB, 58.2 ppm and DPAC*o*OB, 64.8 ppm; vs. DPAC*o*B, 84.0 ppm). As for PLQY, all compounds exhibit high PLQY (0.91–0.99) in oxygen free toluene and largely decrease in air-saturated toluene (≤ 0.06). This effect may indicate quenching of the T_1 state by triplet oxygen, which in turn implies an efficient $T_1 \rightarrow S_1$ reverse intersystem crossing (RISC) in oxygen-free toluene.[9]

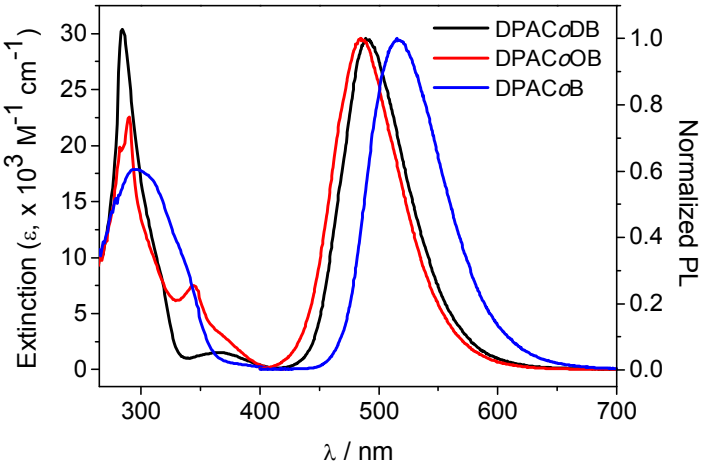

Figure 12. UV/vis absorption (left) and PL spectra (right) of DPAC*o*DB, DPAC*o*OB, and DPAC*o*B toluene (5.0×10^{-5} M) at 298 K.

Table 3. Photophysical properties of DPAC*o*DB, DPAC*o*OB, and DPAC*o*B.

Compound	λ_{abs}[a] [nm]	λ_{PL} [nm]		Φ_{PL} (%)		τ_p [ns (%)][c]	τ_d [μs (%)][d]	
		Toluene[a]	PMMA	Toluene[b] (N_2/air)	PMMA	Toluene	Toluene	PMMA
DPAC*o*DB	284, 366	490	460	91/6	90	62.17 (40)	8.10 (60)	9.12 (65)
DPAC*o*OB	290, 344, 375	485	448	99/6	99	173.37 (52)	8.46 (48)	8.30 (51)
DPAC*o*B	295	516	493	99/5	98	200.68 (13)	8.31 (87)	8.72 (88)

[a)] In oxygen-free toluene at 298 K (5.0×10^{-5} M); [b)] Absolute photoluminescence quantum yields (PLQYs) in oxygen-free (N_2) and air-saturated (air) toluene at 298 K; [c)] PL lifetimes of prompt (τ_p) decay components for the air-saturated toluene solutions at 298 K. The estimated prompt (Φ_{PF}) portions (%) in transient decay curves are given in parentheses. [d)] PL lifetimes of delayed (τ_d) decay components (oxygen-free toluene solutions and film at 298 K). The estimated delayed (Φ_{DF}) portions (%) in transient decay curves are given in parentheses.

Photophysical properties were also measured in spin-coated PMMA film doped with 10% weight (10 wt%) of compounds (**Figure 13**). Similarly cyclic triarylboron shows blue-shifted emission compared to non-cyclic $BMes_2$. However, the blue-shifts of ca. 24–37 nm were observed compared to solution data (i.e. DPAC*o*DB = 460 nm; DPAC*o*OB = 448 nm; DPAC*o*B = 493 nm), and much greater than observed for other *ortho*-D–A compounds.[9, 26] This could be affected from the bulkiness and rigidity of compounds, giving rigidochromism effect towards blue region.[27] All compounds in film also exhibit high PLQY in a value of 0.90–0.99.

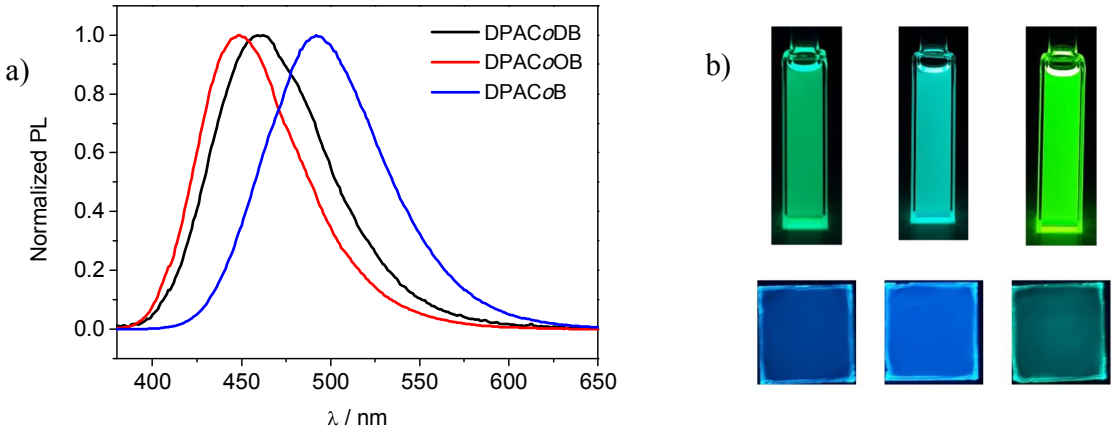

Figure 13. (a) PL spectra of DPAC*o*DB, DPAC*o*OB, and DPAC*o*B in PMMA film 10% weight. (b) Emission color in solution and film illuminated with UV lamp 365 nm.

The transient PL decay curves of all compounds showed two decay components, i.e., the prompt (τ_p) and delayed (τ_d) components at 298 K (**Figure 14** and **Table 3**).[7, 9] All compounds shows similar delay in range of ~8 μs and portion both in solution and film state. To confirm the observed delayed emission can be assigned as TADF, a gradual increase in the emission intensity of the delayed component with increasing temperature from 140 to 290 K also displayed in DPAC*o*OB compound (**Figure 15**). Furthermore, the ΔE_{ST} values were determined experimentally from the fluorescence and phosphorescence spectra at 77 K, and were found to be in the range within and less than 0.02 eV, which

are small enough to explain the characteristic and requirement of TADF compounds (**Figure 16**, **Table 4**).[7, 9]

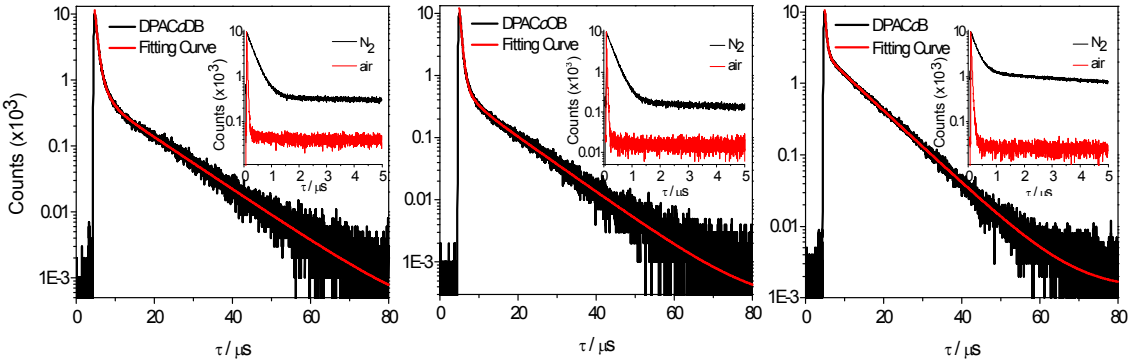

Figure 14. Transient PL decay curves of DPAC*o*DB (left), DPAC*o*OB (middle), DPAC*o*B (right) in oxygen-free toluene at 298 K. The inset shows the decay curves in oxygen-free (N_2) and air-saturated toluene.

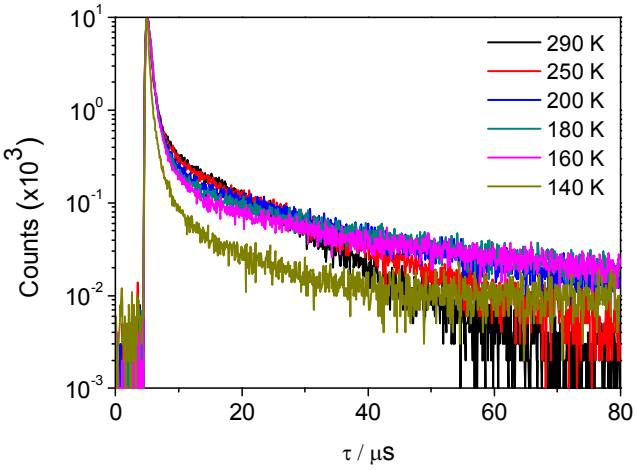

Figure 15. The temperature dependant of the transient PL decay from 140 to 290 K (DPAC*o*OB).

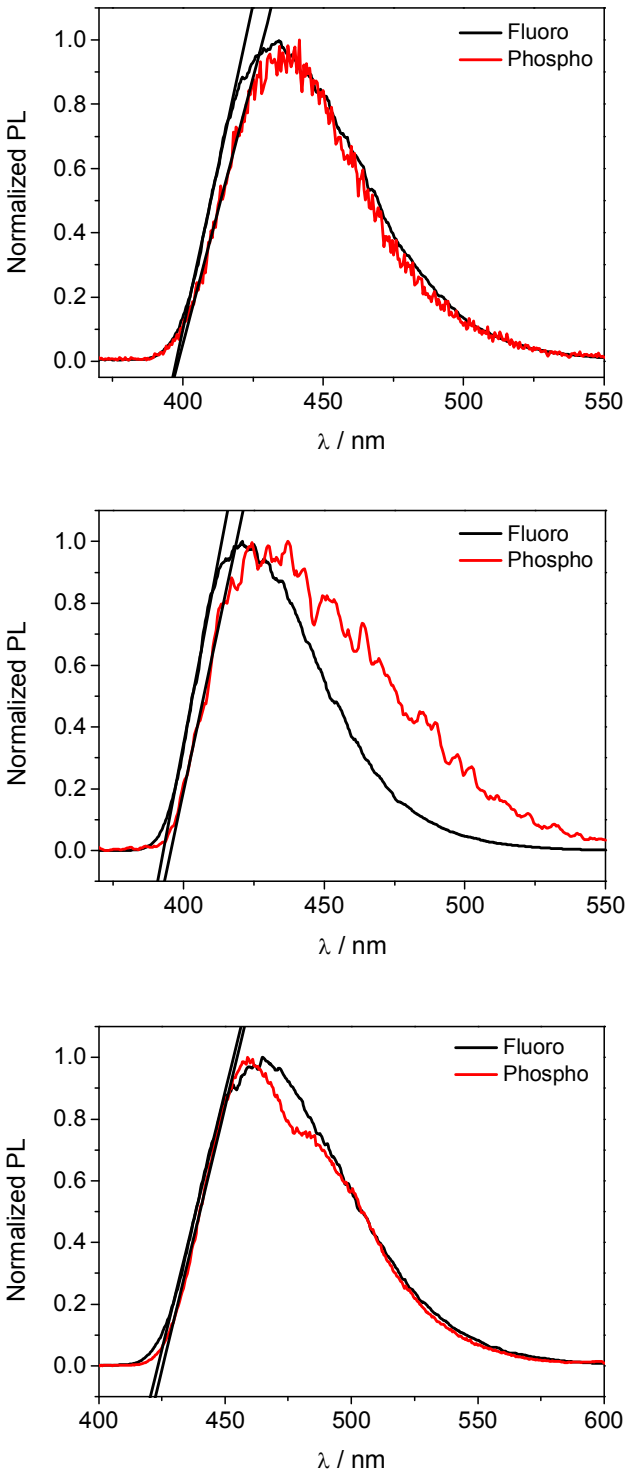

Figure 16. Fluorescence and phosphorescence spectra of DPAC*o*DB (top), DPAC*o*OB (middle), and DPAC*o*B (bottom) in toluene at 77 K.

Table 4. Photophysical data of DPACoDB, DPACoOB, and DPACoB at 77 K.

Compound	λ_{PL} [nm]	E_S/E_T[a] [eV]	ΔE_{ST}[b] [eV]
DPAC*o*DB	433	3.12/3.11	< 0.01
DPAC*o*OB	421	3.16/3.14	0.02
DPAC*o*B	464	2.93/2.92	0.01

[a] E_S and E_T were calculated from the onset of fluorescence and phosphorescence spectra respectively. [b] $\Delta E_{ST} = E_S - E_T$.

3. Electrochemical Properties

To understand the character of the frontier orbitals, the electrochemical properties of DPAC*o*DB, DPAC*o*OB**,** and DPAC*o*B were carried out by cyclic voltammetry (**Figure 17** and **Table 5**). The half-wave oxidation potentials (E_{ox} versus Fc/Fc^{+}) were 0.51 V (DPAC*o*DB), 0.54 V (DPAC*o*OB) and 0.54 V (DPAC*o*B), correspond to the reversible oxidation from donor moieties of diphenylacridine group.[28] Consequently, their HOMO energy levels determined from the half-wave oxidation potentials were –5.31 eV, –5.34 eV, and –5.34 eV respectively. As for reduction, all compounds shows reversible reduction potential due to the same moieties of triarylboron compounds. The cyclic triarylboron acceptor (DPAC*o*OB**,** –2.42 V) tend to have a negatively shifted potential compared to non-cyclic $BMes_2$ (DPAC*o*B, –2.38 V), giving more positive LUMO level. This data can be attributed to the effect of π-donation from cyclic ipso-carbon to boron center. However, though DPAC*o*DB also has cyclic acceptor, its reduction potential is positively charged (–2.32 V) presumably due to the stabilization of the boryl moiety by DMSO solvent. This effect may give rise to the stabilization of LUMO level, thus decreasing energy gap. All reduction potentials estimated from the half-wave reduction potential, giving their calculated LUMO energy levels were –2.48 eV (DPAC*o*DB), –2.38 eV (DPAC*o*OB), and –2.42 eV (DPAC*o*B) respectively.

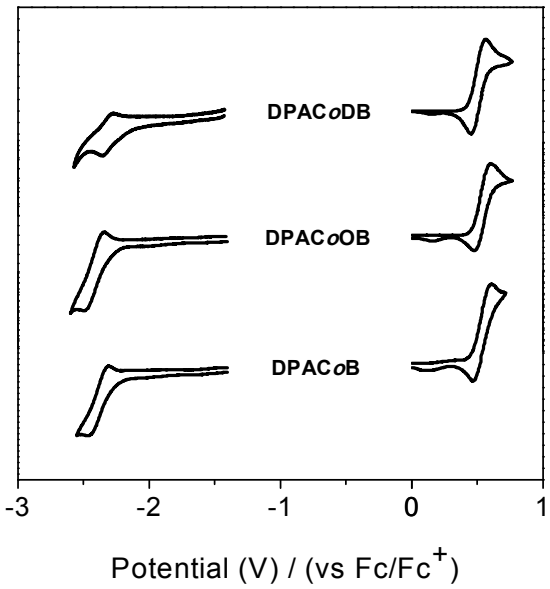

Figure 17. Cyclic voltammograms of DPAC*o*DB, DPAC*o*OB, and DPAC*o*B, showing reduction (left) and oxidation (right).

Table 5. Cyclic Voltammetry Data of DPAC*o*DB, DPAC*o*OB, and DPAC*o*B.

Compound	E_{ox}[a] [V]	E_{red}[b] [V]	HOMO/LUMO [eV]	E_g[d] [eV]
DPAC*o*DB	0.51	–2.32[c]	–5.31/–2.48	2.83
DPAC*o*OB	0.54	–2.42	–5.34/–2.38	2.96
DPAC*o*B	0.54	–2.38	–5.34/–2.42	2.92

[a)] Measured in CH_2Cl_2 (1×10^{-3} M, scan rate = 100 mV/s). [b)] Measured in THF (1×10^{-3} M, scan rate = 100 mV/s). [c)] Measured in DMSO (1×10^{-4} M, scan rate = 200 mV/s). All reversible oxidation and reduction measured with reference to a Fc/Fc^+ redox couple at 298 K. [d)] E_g = LUMO – HOMO.

IV. CONCLUSION

Ortho-donor-appended TADF compounds containing a 9,9-diphenyl-9,10-dihydroacridine (DPAC) donor and different triarylboron acceptors (DPAC*o*DB, DPAC*o*OB, and DPAC*o*B) were successfully synthesized and characterized. All compounds were confirmed to have high quantum yields (0.91–0.99) and small ΔE_{ST} values in oxygen-free toluene solution, which implies strong TADF properties. Furthermore, cyclic acceptors such as boraantrahcene (DPAC*o*DB) and oxaborin (DPAC*o*OB) in *ortho* D-A system tend to increase π-donating effect, leading to blue-shifted PL spectra compared to non-cyclic $BMes_2$ (DPAC*o*B) both in solution and PMMA film. All compounds displayed high thermal stability, making these compounds a good candidate as stable TADF-OLED emitters. The modification of triarylboron moieties would also give a new insight to develop highly efficient stable deep-blue TADF emitters.

V. REFERENCES

1. Pope, M.; Kallmann, H. P.; Magnante, P., Electroluminescence in Organic Crystals. *The Journal of Chemical Physics* **1963,** *38* (8), 2042-2043.

2. Tang, C. W.; VanSlyke, S. A., Organic electroluminescent diodes. *Appl. Phys. Lett.* **1987,** *51* (12), 913-915.

3. Kappaun, S.; Slugovc, C.; List, E. J., Phosphorescent organic light-emitting devices: working principle and iridium based emitter materials. *Int J Mol Sci* **2008,** *9* (8), 1527-47.

4. M. A. Baldo, D. F. O. B., Y. You, A. Shoustikov,; S. Sibley, M. E. T. S. R. F., Highly efficient phosphorescent emission from organic electroluminescent devices. *Nature* **1998,** *395*, 151-154.

5. Yang, Z.; Mao, Z.; Xie, Z.; Zhang, Y.; Liu, S.; Zhao, J.; Xu, J.; Chi, Z.; Aldred, M. P., Recent advances in organic thermally activated delayed fluorescence materials. *Chem. Soc. Rev.* **2017,** *46* (3), 915-1016.

6. Wong, M. Y.; Zysman-Colman, E., Purely Organic Thermally Activated Delayed Fluorescence Materials for Organic Light-Emitting Diodes. *Adv. Mater.* **2017,** *29* (22).

7. Uoyama, H.; Goushi, K.; Shizu, K.; Nomura, H.; Adachi, C., Highly efficient organic light-emitting diodes from delayed fluorescence. *Nature* **2012,** *492* (7428), 234-8.

8. Liu, Y.; Li, C.; Ren, Z.; Yan, S.; Bryce, M. R., All-organic thermally activated delayed fluorescence materials for organic light-emitting diodes. *Nature Reviews Materials* **2018,** *3* (4).

9. Lee, Y. H.; Park, S.; Oh, J.; Shin, J. W.; Jung, J.; Yoo, S.; Lee, M. H., Rigidity-Induced Delayed Fluorescence by Ortho Donor-Appended Triarylboron Compounds: Record-High Efficiency in Pure Blue Fluorescent Organic Light-Emitting Diodes. *ACS Appl Mater Interfaces* **2017,** *9* (28), 24035-24042.

10. Endo, A.; Sato, K.; Yoshimura, K.; Kai, T.; Kawada, A.; Miyazaki, H.; Adachi, C., Efficient up-conversion of triplet excitons into a singlet state and its application for organic light emitting diodes. *Appl. Phys. Lett.* **2011,** *98* (8), 083302.

11. Im, Y.; Kim, M.; Cho, Y. J.; Seo, J.-A.; Yook, K. S.; Lee, J. Y., Molecular Design Strategy of Organic Thermally Activated Delayed Fluorescence Emitters. *Chem. Mater.* **2017,** *29* (5), 1946-1963.

12. Turkoglu, G.; Cinar, M. E.; Ozturk, T., Triarylborane-Based Materials for OLED Applications. *Molecules* **2017,** *22* (9).

13. Chen, X. L.; Jia, J. H.; Yu, R.; Liao, J. Z.; Yang, M. X.; Lu, C. Z., Combining Charge-Transfer Pathways to Achieve Unique Thermally Activated Delayed Fluorescence Emitters for High-Performance Solution-Processed, Non-doped Blue OLEDs. *Angew. Chem. Int. Ed. Engl.* **2017,** *56* (47), 15006-15009.

14. Kitamoto, Y.; Namikawa, T.; Ikemizu, D.; Miyata, Y.; Suzuki, T.; Kita, H.; Sato, T.; Oi, S., Light blue and green thermally activated delayed fluorescence from 10H-phenoxaborin-derivatives and their application to organic light-emitting diodes. *Journal of Materials Chemistry C* **2015,** *3* (35), 9122-9130.

15. Ahn, D. H.; Kim, S. W.; Lee, H.; Ko, I. J.; Karthik, D.; Lee, J. Y.; Kwon, J. H., Highly efficient blue thermally activated delayed fluorescence emitters based on symmetrical and rigid oxygen-bridged boron acceptors. *Nature Photonics* **2019,** *13* (8), 540-546.

16. Kondo, Y.; Yoshiura, K.; Kitera, S.; Nishi, H.; Oda, S.; Gotoh, H.; Sasada, Y.; Yanai, M.; Hatakeyama, T., Narrowband deep-blue organic light-emitting diode featuring an organoboron-based emitter. *Nature Photonics* **2019,** *13* (10), 678-682.

17. Zhou, Z.; Wakamiya, A.; Kushida, T.; Yamaguchi, S., Planarized triarylboranes: stabilization by structural constraint and their plane-to-bowl conversion. *J. Am. Chem. Soc.* **2012,** *134* (10), 4529-32.

18. Mohand Melaimi, S. S., Ching-Wen Chiu, Huadong Wang, and Francois P. Gabbai, Structural and Electrochemical Investigations of the High Fluoride Affinity of Sterically Hindered 1,8-Bis(boryl)naphthalenes. *Inorg. Chem.* **2006,** *45*, 8136-43.

19. Ikeuchi, T.; Inuki, S.; Oishi, S.; Ohno, H., Gold(I)-Catalyzed Cascade Cyclization Reactions of Allenynes for the Synthesis of Fused Cyclopropanes and Acenaphthenes. *Angew. Chem. Int. Ed. Engl.* **2019,** *58* (23), 7792-7796.

20. Lv, J.; Liu, Q.; Tang, J.; Perdih, F.; Kranjc, K., A facile synthesis of indolo[3,2,1-jk]carbazoles via palladium-catalyzed intramolecular cyclization. *Tetrahedron Lett.* **2012,** *53* (39), 5248-5252.

21. Lin, T. A.; Chatterjee, T.; Tsai, W. L.; Lee, W. K.; Wu, M. J.; Jiao, M.; Pan, K. C.; Yi, C. L.; Chung, C. L.; Wong, K. T.; Wu, C. C., Sky-Blue Organic Light Emitting Diode with 37% External Quantum Efficiency Using Thermally Activated Delayed Fluorescence from Spiroacridine-Triazine Hybrid. *Adv. Mater.* **2016,** *28* (32), 6976-83.

22. Wrackmeyer, B., Nuclear Magnetic Resonance Spectroscopy of Boron Compounds Containing Two-, Three- and Four-Coordinate Boron. **1988,** *20*, 61-203.

23. Lee, Y. H.; Park, S.; Oh, J.; Woo, S.-J.; Kumar, A.; Kim, J.-J.; Jung, J.; Yoo, S.; Lee, M. H., High-Efficiency Sky Blue to Ultradeep Blue Thermally Activated Delayed Fluorescent Diodes Based on Ortho-Carbazole-Appended Triarylboron Emitters: Above 32% External Quantum Efficiency in Blue Devices. *Advanced Optical Materials* **2018,** *6* (17), 1800385.

24. Park, I. S.; Lee, J.; Yasuda, T., High-performance blue organic light-emitting diodes with 20% external electroluminescence quantum efficiency based on pyrimidine-containing thermally activated delayed fluorescence emitters. *Journal of Materials Chemistry C* **2016,** *4* (34), 7911-7916.

25. Cheng, Z.; Li, Z.; Xu, Y.; Liang, J.; Lin, C.; Wei, J.; Wang, Y., Achieving Efficient Blue Delayed Electrofluorescence by Shielding Acceptors with Carbazole Units. *ACS Appl Mater Interfaces* **2019,** *11* (31), 28096-28105.

26. Kumar, A.; Oh, J.; Kim, J.; Jung, J.; Lee, M. H., Facile color tuning of thermally activated delayed fluorescence by substituted ortho-carbazole-appended triarylboron emitters. *Dyes and Pigments* **2019,** *168*, 273-280.

27. Lakowicz, J. R., Principles of Fluorescence Spectroscopy, 3rd edition. **2006**.

28. Andrew, T. L.; Swager, T. M., Detection of explosives via photolytic cleavage of nitroesters and nitramines. *J. Org. Chem.* **2011,** *76* (9), 2976-93.